JACS
JOURNAL OF THE AMERICAN CHEMICAL SOCIETY
pubs.acs.org/JACS
Article

Reactivity Prediction of Cu-Catalyzed Halogen Atom Transfer Reactions Using Data-Driven Techniques

Francesca Lorandi,* Marco Fantin,* Hossein Jafari, Adam Gorczynski, Grzegorz Szczepaniak, Sajjad Dadashi-Silab, Abdirisak A. Isse, and Krzysztof Matyjaszewski*

Cite This: J. Am. Chem. Soc. 2023, 145, 21587−21599
Read Online
ACCESS | Metrics & More | Article Recommendations | Supporting Information

ABSTRACT: In catalysis, linear free energy relationships (LFERs) are commonly used to identify reaction descriptors that enable the prediction of outcomes and the design of more effective catalysts. Herein, LFERs are established for the reductive cleavage of the C(sp^3)−X bond in alkyl halides (RX) by Cu complexes. This reaction represents the activation step in atom transfer radical polymerization and atom transfer radical addition/cyclization. The values of the activation rate constant, k_{act}, for 107 Cu complex/RX couples in 5 different solvents spanning over 13 orders of magnitude were effectively interpolated by the equation: $\log k_{act} = s_C(I + C + S)$, where I, C, and S are, respectively, the initiator, catalyst, and solvent parameters, and s_C is the catalyst-specific sensitivity parameter. Furthermore, each of these parameters was correlated to relevant descriptors, which included the bond dissociation free energy of RX and its Tolman cone angle θ, the electron affinity of X, the radical stabilization energy, the standard reduction potential of the Cu complex, the polarizability parameter π^* of the solvent, and the distortion energy of the complex in its transition state. This set of descriptors establishes the fundamental properties of Cu complexes and RX that determine their reactivity and that need to be considered when designing novel systems for atom transfer radical reactions. Finally, a multivariate linear regression (MLR) approach was adopted to develop an objective model that surpassed the predictive capability of the LFER equation. Thus, the MLR model was employed to predict k_{act} values for >2000 Cu complex/RX pairs.

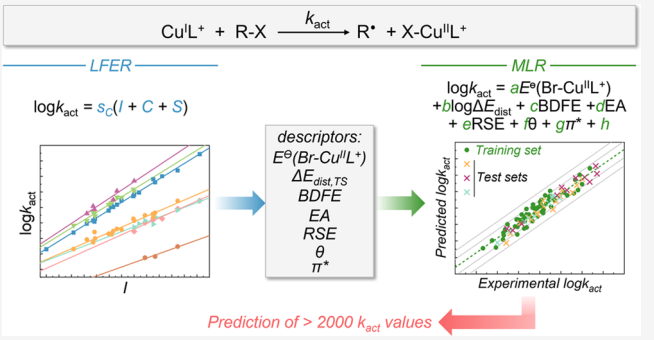

1. INTRODUCTION

The ability to design efficient catalysts and predict the reaction outcomes is a fundamental goal in chemistry. Reaching this goal hinges on rationalizing experimental results through the identification of structure−performance relationships. Scaling relations are key tools in catalysis that enable reducing the complexity of a reaction system.[1,2] In scaling relations, the activation energies of a catalytic cycle are expressed as a function of selected bond energies or descriptors. This facilitates the understanding of the reaction and guides the development of new catalysts, which can be accelerated by combination with machine learning methods.[3,4]

One of the fundamental types of scaling relations is linear free energy relationship (LFER).[1,5] This is linked to the Hammond's postulate,[6] which establishes that the transition state of a reaction resembles the state (reactants or products) to which it is closer in energy. LFERs have been extensively applied in various fields, including heterogeneous and homogeneous catalysis,[1,7−9] and organic, bio-organic, and supramolecular chemistry.[10−12] A notable example is Mayr's reactivity scale that enables to predict the rate constant k of a reaction between a nucleophile and an electrophile, given the nucleophilicity and electrophilicity parameters of the two reaction partners (N and E, respectively) and the nucleophile-specific sensitivity parameter s_N.[12,13] The Mayr−Patz equation, $\log k = s_N(N + E)$, was found to apply to over 1200 nucleophiles and 330 electrophiles, spanning a reactivity range of over 35 orders of magnitude.[14−16] The inherent simplicity of the LFER method is an important strength; however, other data-derived tools have emerged for addressing complex reaction systems, such as multivariate linear regression (MLR) models pioneered by Sigman and co-workers.[17,18]

Catalysis has been playing a crucial role in polymer science since the development of Ziegler−Natta catalysts, metallocene and postmetallocene complexes, Grubbs- and Schrock-type catalysts, and more recently with various catalysts for reversible deactivation radical polymerizations (RDRPs).[19−21] Never-

Received: July 19, 2023
Published: September 21, 2023

theless, the use of LFERs for predicting the outcome of catalyzed polymerizations is uncommon.

Atom transfer radical polymerization (ATRP) is a very effective RDRP technique that enables making well-defined polymer materials with predetermined architectures, which find numerous applications from drug-delivery systems to energy devices.[22−24] The development of ATRP was inspired by metal-catalyzed atom transfer radical addition (ATRA), where a low-oxidation-state transition metal complex reductively cleaves the C(sp^3)−X bond of a small-molecule alkyl halide (RX), generating a radical species and the oxidized form of the metal complex (Scheme 1a). Typically, the generated radical adds to

Scheme 1. Mechanism of Cu-Catalyzed (a) Atom Transfer Radical Addition (ATRA) and (b) Atom Transfer Radical Polymerization (ATRP)

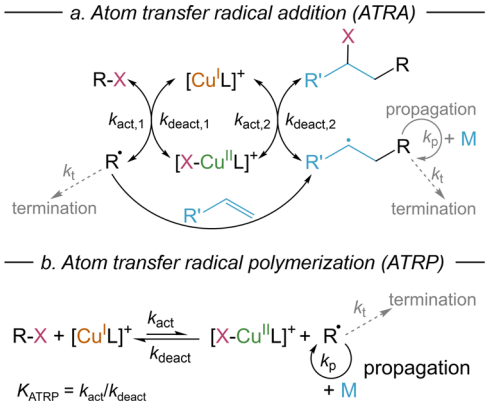

an alkene molecule, forming a new radical that is then quenched by the transfer of X$^\bullet$ from the oxidized metal complex. ATRA, along with its variant forming cyclic adducts (known as atom transfer radical cyclization, ATRC), has become a fundamental reaction in organic chemistry.

ATRP shares the same activation step as ATRA/C. In ATRP, a low-oxidation state Cu complex, $[Cu^IL]^+$ (L = polydentate amine ligand), is utilized as an activator catalyst that reductively cleaves the C(sp^3)−X bond in RX initiators or dormant species to form propagating radicals (Scheme 1b). This activation process occurs via concerted inner-sphere electron transfer and halogen atom transfer (ISET-AT), resulting in the formation of the high-oxidation state, halogenated complex $[X-Cu^{II}L]^+$.[24−26] The latter acts as a deactivator of propagating radicals, regenerating dormant species and $[Cu^IL]^+$, upon the deactivation step.

The rate of polymerization and the precise control over the composition and topology of the (co)polymers made by ATRP depend on the choice of catalyst, alkyl halide initiator, and monomer (which determines the nature of the dormant species). Fundamental parameters that characterize ATRP catalysts and RX initiators or dormant species are accessed through either experimental or computational methods.[25,27−30] These measurements revealed some fundamental correlations that apply to ATRP systems: (i) The logarithm of the ATRP equilibrium constant ($\log K_{ATRP}$) scales linearly with the standard reduction potential, E^Θ, of $[X-Cu^{II}L]^+$ (for a fixed RX, solvent and temperature);[27] (ii) For a fixed halide ion, K_{ATRP} is proportional to the bond dissociation free energy (BDFE) of the C(sp^3)−X bond in the alkyl halide dormant species;[28] (iii) Log K_{ATRP} increases linearly with $\log k_{act}$ for a series of catalysts and RX initiators, in a fixed solvent;[29] (iv) The value of k_{act}, and thus of K_{ATRP}, increases with increasing polarity of the solvent, and this behavior is well described by considering the dipolarity/polarizability parameter π^* of the solvent.[27,31,32]

These correlations guided the design of novel ATRP catalysts, but they were established by analyzing relatively small sets of catalysts, initiators, or solvents. As a result, there is no general theory to understand and predict k_{act}. Moreover, several challenges remain open in ATRP, such as the possibility of polymerizing less activated monomers. Hence, there is a need to identify a simple relationship that comprehensively covers various families of catalysts, initiators/dormant species, and solvents. Although an early attempt to define an LFER for k_{act} in ATRP was reported in 2012, it was never expanded further.[33]

Here, our objective is to develop a comprehensive model for understanding and predicting the rate constant of RX activation by Cu-based complexes, a crucial step in ATRP and small-molecule transformations by ATRA/C. Our methodology is depicted in Scheme 2. First, we compiled an extensive database

Scheme 2. Workflow for Establishing a Comprehensive Model for Reactivity of RX Activation by Cu-Based Catalysts

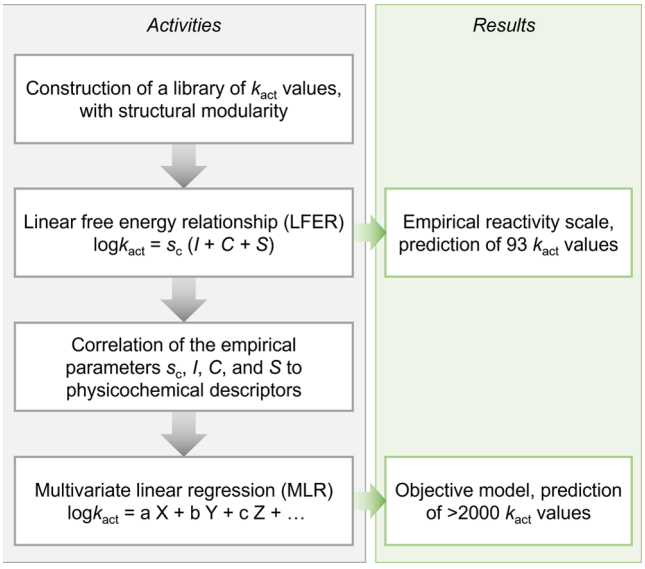

of k_{act} values by integrating the literature data with newly measured data. This approach allowed us to broaden the scope of catalyst and RX reactivity and to include a wider range of initiator structures. This training database comprised k_{act} values for 107 catalyst/RX pairs, encompassing systems from the most active to the least active examined thus far.

Second, we showed that the reactivity of this extensive range of catalyst/RX pairs is described by a simple relationship inspired by the Mayr−Patz equation (eq 1). In this equation, $\log k_{act}$ depends on a set of empirical parameters: an initiator parameter (I), a catalyst parameter (C), and a catalyst-specific sensitivity parameter (s_C). In addition to traditional LFERs, we introduced a solvent parameter (S) to account for the solvent effect on k_{act}.

$$\log k_{act} = s_C(I + C + S) \quad (1)$$

This LFER encompasses 8 different Cu complexes, 25 alkyl halides (Scheme 3), and 5 solvents, covering a range of k_{act} values spanning over 13 orders of magnitude. The empirical value of eq 1 represents a simple relationship for estimating the

https://doi.org/10.1021/jacs.3c07711
J. Am. Chem. Soc. 2023, 145, 21587−21599

Scheme 3. Structures of Ligands and Alkyl Halide Initiators, with the Corresponding Radicals and Monomer Mimics, for Cu-Catalyzed ATRP, Considered in This Work[a34]

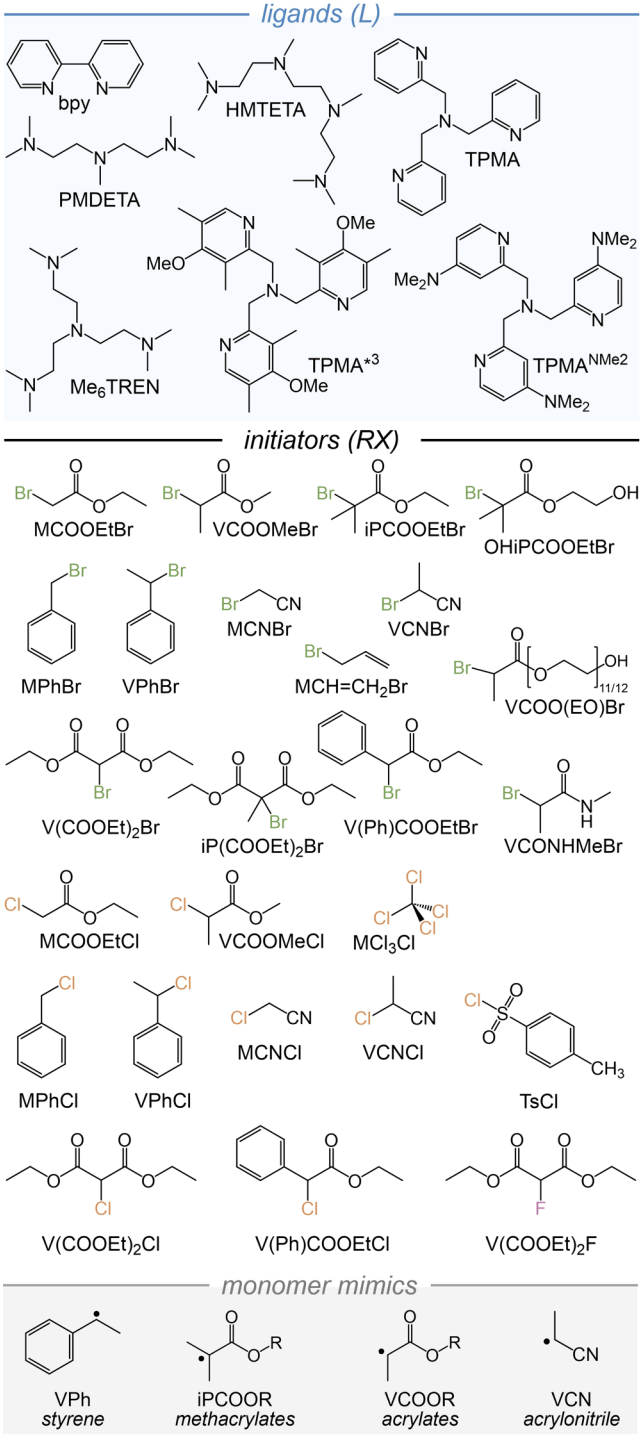

[a]The nomenclature for RX species was adopted from ref 34.

activity of Cu complexes toward alkyl halides in different solvents; specifically, it was used to predict the k_{act} of 93 common catalyst/RX pairs in acetonitrile (ACN), with the potential for hundreds more predictions in other solvents.

Third, aiming to establish a correlation that surpasses the empirical nature of eq 1, each empirical parameter in eq 1 (s_c, C, I, S) was correlated with pertinent physicochemical descriptors such as standard reduction potentials, BDFE, steric parameters, etc. These key experimental and computational descriptors govern the effect of the solvent and the reactivity of both Cu-based catalysts and alkyl halides.

Finally, by employing an MLR approach, we developed a robust equation to determine the k_{act} of RX initiators in different solvents from available experimental and computational descriptors. The MLR provided an objective model with improved predictive capability compared to the LFER, enabling the prediction of k_{act} values for >2000 CuL/RX couples in ACN based on existing experimental and computational data.

2. RESULTS AND DISCUSSION

2.1. Construction of a Library of k_{act} Values.

2.1.1. Selection of k_{act} Data. Construction of an accurate LFER hinges on the establishment of a comprehensive and precise library of k_{act} values. Herein, these values are obtained through a combination of experimental measurements and carefully selected data from the literature sources. To ensure accuracy, the k_{act} values must be determined by studying the reaction between RX and the actual ATRP catalyst, specifically the $[Cu^IL]^+$ complex, under conditions where halide ions are absent. In such conditions, at least one coordination site on the copper ion is either free or occupied by the solvent.[35]

The activation step of ATRP was investigated in several studies.[25,36,37] However, in most of these works, the measurements were conducted in the presence of halide ions, resulting typically in underestimated activation rate constants. To determine k_{act} when halide ions are present, the halidophilicity constant of $[Cu^IL]^+$ and the speciation of Cu^I species must be known (see Tables S2−S6 in the Supporting Information, SI). In the literature, we found k_{act} values for 72 ATRP catalyst/initiator pairs measured in the absence of halide ions and with low error (<15%). These values were determined via electrochemical methods applied to $[Cu^IL]^+$ species (Tables S7 and S8). In general, k_{act} values $<5 \times 10^3$ M^{-1} s^{-1} were determined by chronoamperometry at a rotating disk electrode (RDE), whereas k_{act} values $\geq 5 \times 10^3$ M^{-1} s^{-1} were determined by cyclic voltammetry (CV) with digital simulations.[38,39] The largest portion of available k_{act} values were determined in ACN, focusing on various RBr and RCl, and moderately active Cu complexes, bearing ligands such as tris[2-(dimethylamino)-ethyl]amine (Me_6TREN), tris(2-pyridylmethyl)amine (TPMA), and *N,N,N′,N″,N″*-pentamethyldiethylenetriamine (PMDETA).[29]

Nevertheless, the existing literature lacked a satisfactory reactivity scope and structural modularity, necessitating the experimental measurement of k_{act} values for 35 new Cu catalyst/RX pairs. The selection of these pairs was based on two criteria: (i) expanding the reactivity scope, including both low-activity Cu catalysts and highly reactive RX initiators bearing weak C(sp^3)−X bonds and (ii) expanding the structural modularity of the initiators by including a larger variety of initiator structures, comprising several trisubstituted halides (e.g., halo methyl malonates) and monosubstituted halides (e.g., allyl halides). The whole set of new as well as literature data are collected in Tables S7 and S8. All new k_{act} values (35) were determined by established electrochemical methods as described in Section S1 in the SI.

It should be noted that k_{act} values considered in this work were determined either at 25 °C or room temperature. The effect of temperature on k_{act} was previously analyzed on some catalyst/RX pairs, and an increment in k_{act} of a factor of ∼2 every 20 °C was determined.[25,40]

https://doi.org/10.1021/jacs.3c07711
J. Am. Chem. Soc. 2023, 145, 21587−21599

2.1.2. Broadening the Scope of Initiators. To expand the range of k_{act}, more reactive initiators were investigated in combination with the catalyst $[Cu^{I}TPMA]^{+}$. We selected 2-bromopropionitrile (VCNBr) as an initiator mimicking the dormant species of acrylonitrile. Additionally, we selected diethyl bromomalonate ($V(COOEt)_2Br$) and diethyl 2-methyl-2-bromomalonate ($iP(COOEt)_2Br$) as initiators, the latter mimicking methylene malonate monomers. These monomers are highly reactive, although sterically hindered, and their controlled polymerization by ATRP has not been investigated yet. Nevertheless, bromomalonates are often employed as initiators, particularly for organocatalyzed ATRP reactions.[41] Ethyl α-bromophenylacetate (V(Ph)COOEtBr) was included as it is typically used as an initiator for the ATRP of methacrylates, being the most reactive alkyl bromide known to date. Regarding chloride initiators, ethyl α-chlorophenylacetate (V(Ph)COOEtCl) was also studied, together with carbon tetrachloride (MCl_3Cl) and tosyl chloride (TsCl), which were used as highly active initiators in ATRP and ATRA systems.[42,43] Interestingly, TsCl was the most reactive among all RX analyzed herein, with $k_{act} = 7.3 \times 10^8$ M^{-1} s^{-1} (by Cu/TPMA in ACN), two orders of magnitude higher than for V(Ph)COOEtBr ($k_{act} = 5.7 \times 10^6$ M^{-1} s^{-1}).

This pool of initiators is highly diverse not only in terms of reactivity but also considering steric factors, ranging from rather compact molecules, such as VCNBr and MCl_3Cl, to molecules with more bulky substituents, such as malonates.

Alkyl fluoride chain ends are nearly unexplored in ATRP due to the high strength of the $C(sp^3)$−F bond.[44,45] The activation of an alkyl fluoride initiator, diethyl fluoromalonate ($V(COOEt)_2F$), by Cu/TPMA was measured to expand the k_{act} range to lower values and to test whether RF initiators could be included in LFERs.

2.1.3. Broadening the Catalyst Scope. Catalysts with relatively low ATRP activity, such as Cu/2,2′-bipyridine (bpy) and Cu/1,1,4,7,10,10-hexamethyltriethylenetetramine (HMTETA), were investigated. These Cu complexes have been commonly employed as catalysts for normal ATRP, i.e., without activator regeneration.[33,42,46] Regarding catalysts with high activity, Cu/tris([(4-methoxy-2,5-dimethyl)-2-pyridyl]methyl)amine (TPMA*[3]) was also studied as it is one of the most active ATRP catalysts reported to date.[47]

In addition, the activity of Cu bromide salts (without amine ligands) toward RX was investigated for the first time. Cu halide salts are catalysts with low reactivity that were employed in seminal ATRA systems and remain common in ATRA/C reactions.[48,49] Moreover, they have been recognized as inhibitors or retarders in conventional radical polymerization.[50] Due to their low reactivity, Cu halide salts may be a good match for the ATRP of new classes of very reactive monomers (e.g., cyanoacrylates or methylene malonates). Additionally, their use can largely reduce the cost of ATRP because the amine-based ligand is generally the most expensive component in the system.

First, the thermodynamic properties of Cu/X (X = Cl or Br) in ACN were analyzed by CV (Figure S5). The voltammograms showed a rather complex pattern, with signals continuously shifting to more negative potentials upon adding increasing amounts of X^-, indicating that complexes with different numbers of X^- ligands were present in solution, as previously shown by Bortolamei et al.[51] Nevertheless, all Cu/Br complexes were found to be very weak reducing agents, with a range of reduction potential that was at least 0.5 V more positive than the E^{Θ} of $[Br-Cu(bpy)_2]^+$ (0.02 V vs SCE).[27] According to the relationship between K_{ATRP} and E^{Θ}, this would suggest that Cu/Br is ca. 8 orders of magnitude less active in ATRP than Cu/bpy. We estimated E^{Θ} for the Cu/Br system as described in Section S2.2 in the SI, obtaining $E^{\Theta} = 0.49$ V vs SCE.

Due to the expected low activity of Cu/Br systems and the complexity of their voltammetric pattern, UV−vis spectrometry was a more appropriate technique than electrochemical tools to measure k_{act}. The conditions were adjusted as described in Section S2.2 in the SI to account for the complicated speciation of Cu^{I}/Br and Cu^{II}/Br systems and the presence of side reactions. Values of k_{act} of Cu/Br with 3 selected RBr initiators were determined (Table S7).

2.2. Linear Free Energy Relationships. *2.2.1. Construction of Linear Free Energy Relationships.* The assembled library of k_{act} values spanned over 13 orders of magnitude (from $\sim 10^{-5}$ to $\sim 10^{9}$ M^{-1} s^{-1}). It comprised 8 Cu complexes, 25 RX (14 RBr, 10 RCl, 1 RF), and 5 solvents: ACN, *N*,*N*-dimethylformamide (DMF), dimethyl sulfoxide (DMSO), water, and the ionic liquid 1-butyl-3-methylimidazolium trifluoromethanesulfonate ([BMIm][OTf]).

Inspired by the Mayr−Patz equation, we proposed that empirical eq 1 could fit the k_{act} data. We assigned the values of $I = 0$ and $s_C = 1$ to iPCOOEtBr and Cu/TPMA, respectively, and $S = 0$ to ACN. By employing least-squares regression, the experimental log k_{act} values were fitted to eq 1 in order to obtain the *I*, *C*, *S*, and s_C parameters, and the obtained values are listed in Table 1. Details on the regression procedure are provided in Section S1.2 in the SI. When log k_{act} was plotted against the *I* parameter, linear relationships were observed within the explored reactivity range. Figure 1a shows the linear relationships obtained for catalyst/RX couples in ACN. On the right side of the graph, we can see the most active initiators, namely, TsCl and V(Ph)COOEtBr, while on the left side, we

Table 1. Values of the Initiator Parameter *I*, Catalyst Parameter *C*, Sensitivity Parameter s_C, and Solvent Parameter *S* Obtained from eq 1, for the Corresponding RX (X = Br, Cl, F), Cu/L Complexes, and Solvents

RBr	*I*	RCl, RF	*I*
V(Ph)COOEtBr	3.462	TsCl	5.227
$iP(COOEt)_2Br$	2.227	V(Ph)COOEtCl	1.528
$V(COOEt)_2Br$	1.669	MCl_3Cl	1.490
VCNBr	0.856	$V(COOEt)_2Cl$	0.394
iPCOOEtBr	0	VCNCl	−1.667
HOiPCOOEtBr	0	MCNCl	−2.033
MCNBr	−0.061	VCOOMeCl	−3.164
VPhBr	−1.007	VPhCl	−3.116
VCOOMeBr	−1.374	MPhCl	−3.777
VCOO(EO)Br	−1.374	MCOOEtCl	−4.832
MPhBr	−1.803	$V(COOEt)_2F$	−6.998
$MCH{=}CH_2Br$	−1.843		
VCONHMeBr	−2.109		
MCOOEtBr	−3.275		

L	*C*	s_C	solvent	*S*
TPMA*[3]	4.948	1.073	[BMIm][OTf]	0.639
Me_6TREN	4.476	0.999	ACN	0
TPMA	3.595	1	DMF	1.159
PMDETA	0.236	0.698	DMSO	1.610
HMTETA	−0.793	0.622	H_2O	2.846
bpy	−1.100	0.722		
Br	−8.839	0.577		

https://doi.org/10.1021/jacs.3c07711
J. Am. Chem. Soc. 2023, 145, 21587−21599

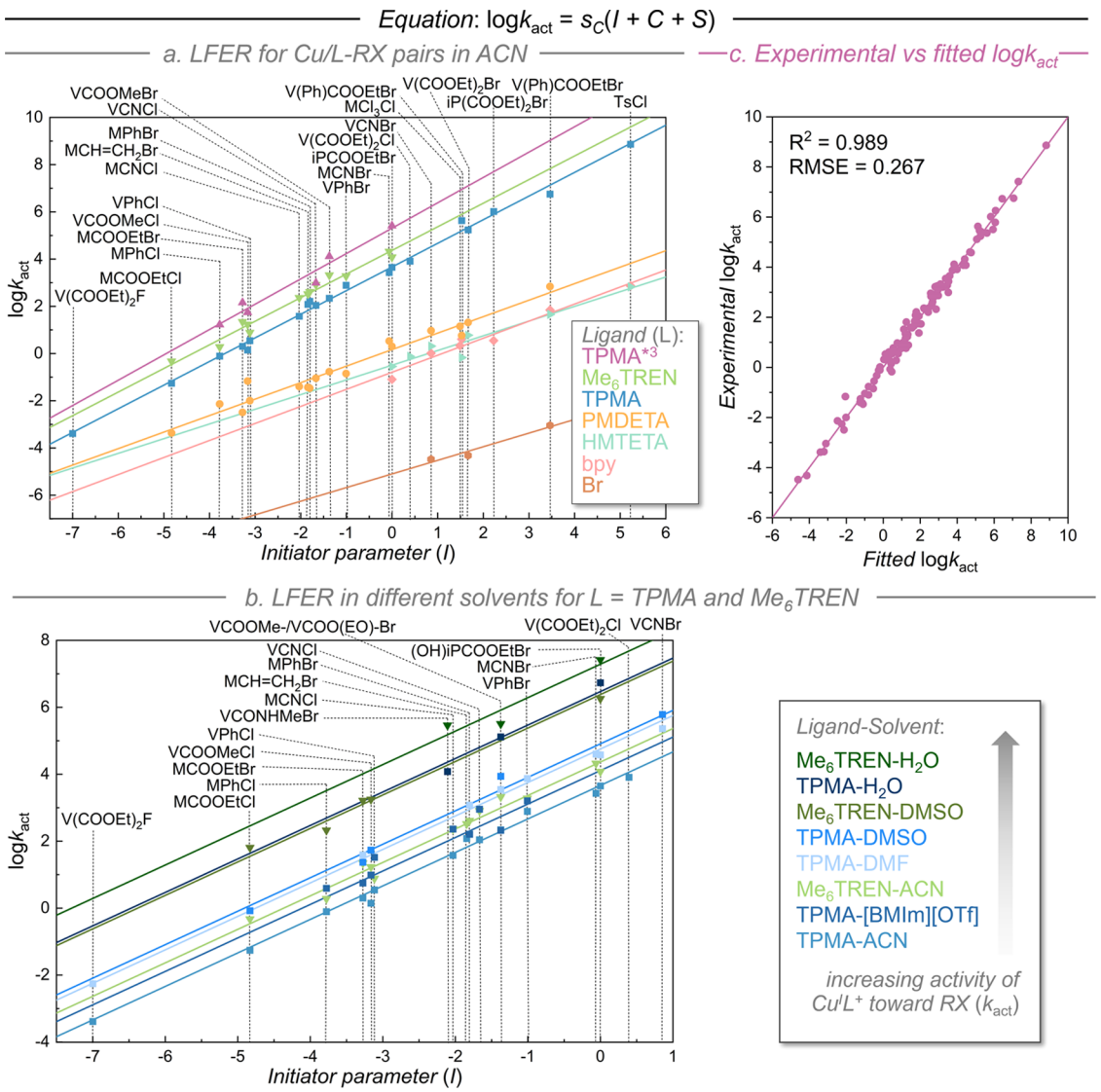

Figure 1. Linear free energy relationships (fitted to eq 1) for a set of ATRP catalyst/initiator pairs in (a) ACN and (b) various solvents. (c) Overall correlation between predicted and experimental log k_{act} values.

have the least active initiator, i.e., the only alkyl fluoride that was investigated. The topmost straight line represents the most active catalyst, Cu/TPMA*[3], while the bottom line corresponds to the least active system, Cu/Br without amine ligands.

Figure 1b shows the LFERs for Cu/TPMA and Cu/Me_6TREN in different solvents, with various RX. Here, the topmost line corresponds to water, while the bottom line represents ACN. The complete set of LFERs, which includes all 107 pairs, is shown in Figure S11.

Additionally, Figure 1c presents the overall comparison between experimental and fitted log k_{act} values based on eq 1. The linear correlation was excellent with R^2 = 0.989 and root-mean-square error (RMSE) = 0.267.

It should be noted that for typical Cu complexes and initiators employed in ATRP, the diffusion limit for the second-order activation reaction corresponds approximately to log k_{act} = 9.5 in ACN (see Section S3.2 in the SI). While the maximum value measured in ACN was log k_{act} = 8.9 (for the activation of TsCl by $[Cu^{I}TPMA]^{+}$), it is reasonable to anticipate that the straight lines in Figure 1 would deviate from linearity in the region above log k_{act} ~ 9, but this was not yet explored by experiments.

2.2.2. Prediction of Log k_{act} Values. The predictive power of eq 1 was assessed by dividing the data set into a training set of 83 values and a validation set of 24 values (Figure S12). The performance of eq 1 in predicting the log k_{act} values of the validation set was found to be remarkable. Consequently, eq 1 was utilized to calculate 93 previously unknown values of log k_{act}, corresponding to all of the missing Cu/L-RX pairs in Figure 1. The calculated values are reported in italics in Tables S13 and S14. Furthermore, numerous additional log k_{act} values can be calculated for different solvents by using appropriate S values for [BMIm][OTf], DMF, DMSO, and water (Table 1).

Subsequently, with the aim of overcoming the empirical nature of eq 1, we explored each parameter (I, C, S, and s_C) to establish correlations with relevant physicochemical descriptors.

2.3. Correlation of Empirical Parameters with Physicochemical Descriptors. *2.3.1. Initiator Parameter (I).* The initiator parameter I is associated with the activity of the alkyl halides, and specifically the dissociative one-electron transfer to the C(sp^3)–X bond (eq 2), which is a crucial step for the activation process.[27]

$$RX + e^{-} \rightleftharpoons R^{\bullet} + X^{-} \quad (2)$$

https://doi.org/10.1021/jacs.3c07711
J. Am. Chem. Soc. 2023, 145, 21587−21599

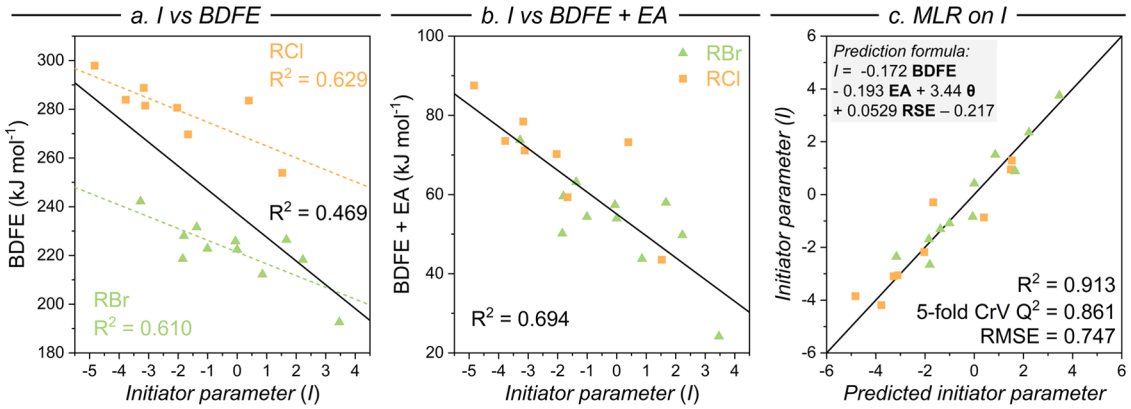

Figure 2. Linear correlation between the initiator parameter I and (a) BDFE or (b) the sum of BDFE and EA. (c) MLR of the initiator parameter I, including the influence of BDFE, EA, radical stabilization energy (RSE), and Tolman cone angle θ on I, for RCl (orange) and RBr (green) ATRP initiators.

From a thermodynamic point of view, this electron transfer can be expressed as the sum of the following two reactions (the thermodynamic parameter of interest is indicated in the same line)

$$RX \rightleftharpoons R^{\bullet} + X^{\bullet} \quad \text{BDFE} \tag{3}$$

$$X^{\bullet} + e^{-} \rightleftharpoons X^{-} \quad \text{EA} \tag{4}$$

where BDFE is the bond dissociation free energy of RX and EA is the electron affinity.

The parameter I was found to correlate linearly but poorly (R^2 = 0.464) with BDFE alone (solid black line in Figure 2a). BDFE values were previously determined for several ATRP initiators in ACN by density functional theory (DFT).[34] (Note: For MCOOEtX, iPCOOEtBr, and V(Ph)COOEtX, BDFEs of the corresponding methyl esters were employed.) The value of I increased with decreasing BDFE of the alkyl halide.

Better correlations were obtained when considering separately RCl and RBr, owing to the different EA of the two halogen atoms (dashed lines in Figure 2a). The plot of BDFE vs I gives two straight lines with similar slopes, one for RBr and one for RCl, the latter shifted to higher BDFE values, due to the higher strength of the C(sp^3)−Cl bond (ca. 40 kJ mol ^{−1} higher for RCl vs the corresponding RBr).

The electron affinity of halogen atoms in ACN was calculated from literature data as EA = −168.44 kJ mol^{-1} and −210.37 kJ mol^{-1} for Br and Cl, respectively (Section S3.3 in the SI). When the I parameters of both RCl and RBr are plotted against the sum of BDFE and EA, all points fall on a single straight line, as shown in Figure 2b. However, the quality of the fit is moderate (R^2 = 0.644) and there are noticeable outliers such as allyl bromide ($MCH{=}CH_2Br$) and malonate-based RX ($V(COOEt)_2Br$, $iP(COOEt)_2Br$, and $V(COOEt)_2Cl$). This suggested that the two thermodynamic descriptors, BDFE and EA, could not completely explain the trend of initiator parameter I.

In order to provide a comprehensive understanding of the initiator parameter I and to gain deeper insights into the behavior of RX in the transition state of the ATRP activation reaction, we expanded the range of descriptors beyond BDFE and EA. In a study by Coote et al., various electronic parameters were calculated for a wide range of alkyl halides, including EA, as well as the ionization potential (IP) of $R^{\bullet}$ and the radical stabilization energy (RSE) of $R^{\bullet}$.[34] Furthermore, a steric factor, the Tolman cone angle (θ) of RX, was calculated to provide a direct measure of the steric crowding around the reaction center (Figure 3a and Table 2).[52] The Tolman cone angle was originally defined for use in inorganic chemistry, as it measures the steric bulk around the central atom in a coordination complex, thus providing information about the accessibility of the central atoms for chemical reactions. For alkyl halides used as polymerization initiators, the calculation of θ was found to be largely independent on the nature of X,[52] providing an effective measure of the steric bulk around the attacking radical. All the available descriptors can be found in Table S9. Considering the diverse set of features that can potentially influence the RX reactivity parameter I (such as BDFE, EA, IP, RSE, and θ), we determined that a multidimensional correlation would be appropriate to account for these factors.

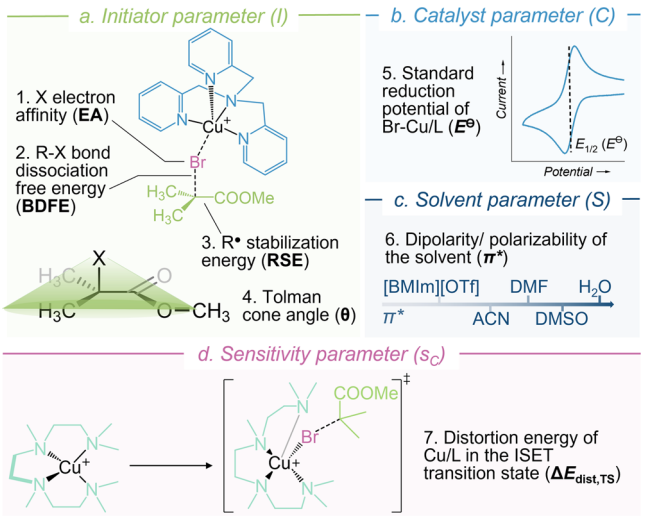

Figure 3. Graphical representation of the parameters in eq 1 and their physicochemical descriptors.

Multivariate linear regression of the I parameter indicated that, in addition to BDFE and EA, RSE and the Tolman cone angle θ were significant descriptors, all statistically significant at the $p \leq 10^{-3}$ value (Table 3). The model yielded the prediction formula in eq 5, with R^2 = 0.913 (Figure 2c).

https://doi.org/10.1021/jacs.3c07711
J. Am. Chem. Soc. 2023, 145, 21587−21599

Table 2. Summary of the Identified Physicochemical Descriptors, Their Meaning, and the Literature References Where Their Values and Determination Procedures Are Reported

	descriptor	description	reaction/detailed description	system component	refs	determination method
1.	EA	electron affinity	$X^{\bullet} + e^{-} \rightleftharpoons X^{-}$	RX	this work	calculation
2.	BDFE	bond dissociation free energy	$RX + e^{-} \rightleftharpoons R^{\bullet} + X^{-}$	RX	34	computational
3.	RSE	radical stabilization energy	extent of delocalization of the unpaired electron in a radical	RX	34,52	computational
4.	θ	Tolman cone angle	the solid angle formed with X at the vertex of a cone and the outermost edge of the van der Waals spheres of the groups in the R fragment at the perimeter of the base of the cone	RX	34,52	computational
5.	E^{Θ}	standard reduction potential of $[Br-Cu^{II}L]^{+}$	$[Br-Cu^{II}L]^{+} + e^{-} \rightarrow [Br-Cu^{I}L]$	$[Br-Cu^{II}L]^{+}$	46, this work	cyclic voltammetry
6.	π^*	dipolarity/polarizability of the solvent	ability of the solvent to stabilize a charge or dipole by virtue of its dielectric effect	solvent	27	spectroscopy
7.	$\Delta E_{dist,TS}$	distortion energy of the catalyst in the transition state	distortion energy of the CuL catalyst in the ISET transition state with respect to the ground state $[Cu^{I}L]^{+}$	$[Br-Cu^{II}L]^{+}$	30	computational

$$I = -0.172 \times \text{BDFE (kJ mol}^{-1}) - 0.193 \times \text{EA (kJ mol}^{-1}) + 3.44 \times \theta \text{ (rad)} - 0.0529 \times \text{RSE (kJ mol}^{-1}) - 0.217 \quad (5)$$

Table 3. Percent Contributions and *p*-Values for the Model Describing *I*

descriptor	% contribution	*p*-value
BDFE (kJ mol^{-1})	57	$<10^{-5}$
EA (kJ mol^{-1})	25	$<10^{-5}$
RSE (kJ mol^{-1})	10	10^{-3}
θ (rad)	8	10^{-3}

A factor intercorrelation analysis indicated that the four factors were not correlated with each other (Figure S13). To test the statistical soundness of the model, a 5-fold cross-validation (CrV) was repeated 20 times with an acceptable average Q^2 = 0.867.

Table 3 presents the percent contribution of each fitted descriptor to the prediction formula for the initiator parameter *I* (the percent contributions were calculated as previously described).[34] The descriptors with the highest percent contribution were BDFE and EA, which align with eqs 3 and 4 that describe their involvement in the thermodynamics of the ATRP equilibrium.

The newly added descriptors, RSE and θ, accounted for 10 and 8%, respectively. Both RSE and θ are associated with the contribution of the R group to k_{act}, and thus to the energy of the transition state. The positive contribution of RSE indicates that R groups that better stabilize the radical lead to higher *I*, and thus higher k_{act}.

Upon initial observation, the contribution of θ may appear counterintuitive. As *I* increases with θ, it suggests that a higher steric crowding around the transition state results in faster reactions. However, recent findings by our groups support the notion that higher reactivity is observed with RX having a larger footprint. Indeed, it has been demonstrated that a strong electrostatic attraction between the R group and L in the transition state actually leads to faster reactions.[30] This suggests that a larger R fragment can have more opportunities to interact with L, leading to a higher *I* and thus a higher k_{act}. This finding also aligns with the concept of the "penultimate effect",[53,54] where the reactivity of macroinitiators is generally higher than that of the corresponding monomeric initiators.

2.3.2. Catalyst Parameter (C). A linear correlation was observed between the catalyst parameter *C* and the standard reduction potential E^{Θ} of the $[Br-Cu^{II}L]^{+}$ complexes measured in ACN (Figure 4a). E^{Θ} is typically measured as the half-wave

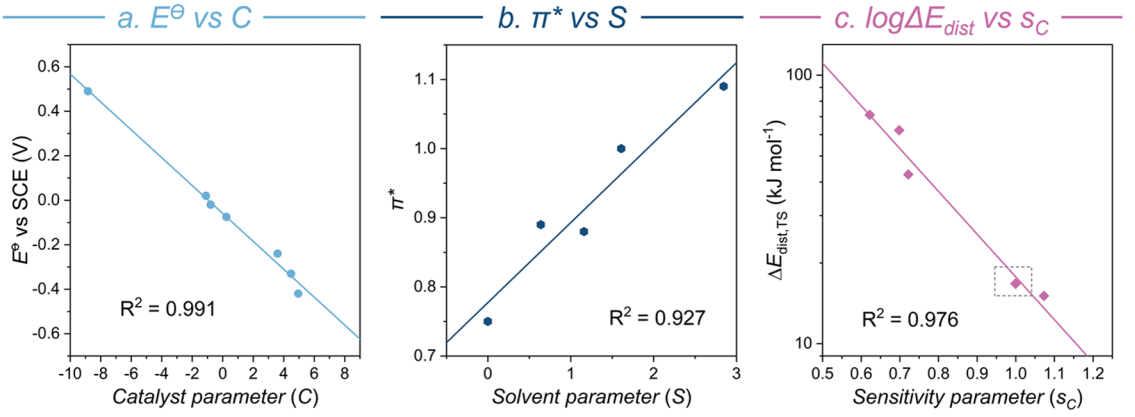

Figure 4. Correlation between (a) E^{Θ} (i.e., $E_{1/2}$) of $[Br-Cu^{II}L]^{+}$ complexes measured in ACN and the corresponding catalyst parameter *C*; (b) polarizability π^* of the solvent and the solvent parameter *S*; (c) distortion energy $\Delta E_{dist,TS}$ (computed in ACN) of Cu/L complexes and the catalyst-specific slope parameter s_C. The dashed square indicates two overlapped points.

https://doi.org/10.1021/jacs.3c07711
J. Am. Chem. Soc. 2023, 145, 21587−21599

potential, $E_{1/2}$, in the CV, Figure 3b. E^{Θ} values of Cu-amine complexes are reported in the literature,[27,45] whereas the E^{Θ} value for the Cu/Br system was estimated in this work (see Section S2.2). The value of C increased as E^{Θ} shifted toward more negative potentials, i.e., when the catalyst is a stronger reducing agent. Overall, C ranged from ca. − 8 to +5, while E^{Θ} varied from 0.49 V vs SCE for $CuBr_2$ to −0.42 V vs SCE for Br−Cu/TPMA*.[3] In summary, $E_{1/2}$ served as a straightforward descriptor for the catalyst parameter C, and the general formula for predicting C is

$$C = -15.9 \times E^{\Theta}([\mathrm{Br} - \mathrm{Cu^{II}L}]^{+})(\mathrm{V\ vs\ SCE}) - 0.949 \quad (6)$$

2.3.3. Solvent Parameter (S). The solvent parameter S was found to exhibit a linear correlation with the dipolarity/polarizability parameter of the solvent, denoted as π^* (Figure 4b). Values of π^* are found in the literature.[27] The value of S increased with increasing polarity of the solvent, in the order [BMIm][OTf] < ACN < DMF < DMSO < H_2O (Figure 3c). The S parameter was a simple addition to the LFER compared with traditional two-parameter LFER equations. Its role was to shift the linear fitting lines upward when the solvent polarity increases (i.e., higher log k_{act}) and downward when it decreases (i.e., lower log k_{act}), compared with the reference solvent (ACN). The general formula for predicting S is

$$S = 8.621 \times \pi^* - 6.698 \quad (7)$$

2.3.4. Sensitivity Parameter (s_C). Finally, we focused on understanding the physicochemical meaning of the slope parameter, which is often the least understood parameter, even for well-established LFERs, such as the nucleophilicity and electrophilicity scales developed by Mayr and colleagues. In our collected data, s_C varied from 0.62 for Cu/HMTETA to 1.07 for Cu/TPMA*[3] (Table 1). s_C is a catalyst-specific parameter and therefore it can depend on several aspects that are known to affect the ATRP activity of Cu complexes.[27,30] Consequently, the following descriptors were considered, which are all available in the literature for many Cu complexes:[30] (i) the electronic properties of the complex, in particular the energy of the highest occupied molecular orbital, E_{HOMO}; (ii) the halogenophilicity (i.e., halogen affinity) of the Cu^{II} complex; (iii) the steric hindrance of L, in particular the percent buried volume of the ligand; (iv) the distortion energy of the Cu/L complex in the ISET transition state (TS) with respect to the ground state $[Cu^{I}L]^{+}$, i.e., $\Delta E_{dist,TS}$, which is an appropriate descriptor for the flexibility of the ligand L. Upon considering the parameters available in the literature (listed in Figure S14), an excellent linear correlation was found between s_C and $\Delta E_{dist,TS}$ of the Cu complexes (Figure 4c). The fitting yielded the following equation

$$s_C = -0.622 \times \log \Delta E_{dist,TS} + 1.776 \quad (8)$$

$\Delta E_{dist,TS}$ of a series of common ATRP catalysts was determined by DFT calculations as the energy difference between the catalyst in its fully optimized ground-state geometry and the same catalyst in its distorted transition state geometry.[30] It was found that the relatively low activity of Cu complexes with flexible ligands (the example for L = HMTETA is shown in Figure 3d) could be explained by their high $\Delta E_{dist,TS}$, in comparison to Cu complexes with more rigid ligands, which had a lower $\Delta E_{dist,TS}$ and higher activity.

The reported values of $\Delta E_{dist,TS}$ for Cu/bpy, Cu/HMTETA, Cu/PMDETA, Cu/TPMA, Cu/Me_6TREN, and Cu/TPMA*[3] were employed to construct the graph in Figure 4c. Complexes with larger $\Delta E_{dist,TS}$ values resulted in lower values of s_C. Cu complexes with tripodal tetradentate ligands (TPMA, TPMA*[3], and Me_6TREN) exhibited lower values of $\Delta E_{dist,TS}$ (i.e., lower flexibility of L) and resulted in high and similar s_C values (∼1). Conversely, flexible tridentate and linear tetradentate ligands exhibited larger values of $\Delta E_{dist,TS}$, resulting in smaller slopes (s_c ∼ 0.7). The relatively low value of s_C for Cu/Br (s_C = 0.58) suggests that $[Cu^{I}Br_2]^{-}$ (likely the active species in Cu/Br systems, as discussed in Section S2.2), has high distortion energy in the TS. This observation aligns with the flexible nature of small Br^{-} ligands and with a significant configuration change upon reaching the TS. According to the correlation in Figure 4c, if $\Delta E_{dist,TS}$ is not available for a certain Cu/L, its s_C can be approximated to a value of 1.0 if L has a tripodal structure, and as 0.7 for all other ligands.

Since s_c is the slope parameter, the LFER analysis reveals that there is a multiplicative (or interaction) effect between $\Delta E_{dist,TS}$ and the reactivity of RX initiators: When reacting with highly active initiators, complexes with more rigid ligands (low $\Delta E_{dist,TS}$) are relatively more active than complexes with flexible ligands. This can be appreciated in Figure 1a, where the fit line for Cu/bpy (relatively rigid ligand) crosses the fit line of Cu/HMTETA (flexible ligand); thus, Cu/bpy becomes more active than Cu/HMTETA for highly reactive RX. This reactivity trend inverts by moving from highly reactive initiators to less reactive ones, for which complexes with more flexible ligands (high $\Delta E_{dist,TS}$) are relatively more active. This observation is important to guide the design of novel catalysts that match the reactivity of targeted monomers (i.e., RX dormant species).

2.3.5. Application of LFER to New Cu/L Catalysts. The definition of a comprehensive relationship that describes the activity of Cu/L complexes toward the reductive cleavage of $C(sp^3)$−X bonds and the determination of the reaction descriptors has two important consequences: (i) the ability to predict currently unknown log k_{act} values of catalyst/RX pairs; (ii) the possibility to guide the design of new L for more active catalysts, which is a challenging, long-standing goal in ATRP. The identified physicochemical descriptors are summarized in Figure 3 and Table 2, together with the literature references that provide their values and detailed description of the computational or experimental methods for their determination. If novel catalysts, RX, or different solvents are considered for log k_{act} prediction, we expect that the use of the reported procedures for descriptors' determination will ultimately provide more accurate log k_{act} values.

The set of eqs 5−8 enables estimation of s_C, C, I, and S and therefore application of LFER eq 1 to new catalysts or RX. As an example, we considered a series of recently developed highly active Cu catalysts for ATRP.[45,55] The ligands in these Cu complexes are structurally analogous to TPMA, except that different electron donating groups (dimethylamino: NMe_2, pyrrolidine: pyr, piperidine: pip, morpholine: mor, Figure 5a) are placed in the *para* position on the aromatic rings. The application of eqs 5−8 and the subsequent use of eq 1 provided values of log k_{act} that were in good agreement with experimental values (Figure 5b and Table S12), with an average error of 0.3 log unit. Additional details on the calculations are given in Section S3.7.

2.3.6. Development of a Comprehensive Model for Predicting k_{act} Values. By substitution of eqs 5−8 into eq 1, an overall predictive equation for log k_{act} can be derived

https://doi.org/10.1021/jacs.3c07711
J. Am. Chem. Soc. 2023, 145, 21587−21599

a. TPMA^R

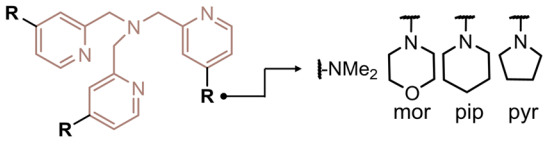

b. Calculated vs experimental logk_{act} for the activation of iPCOOEtBr (I = 0) by Cu/TPMA^R complexes in ACN (S = 0)

R	E^{Θ}([Br–Cu^{II}L]$^+$) (V vs SCE)	C	$\Delta E_{dist,TS}$ (kJ mol^{-1})	s_C	logk_{act} = s_C(I + C + S)	Exp logk_{act}
NMe_2	-0.552	7.83	15.48	1.04	8.1	8.6
pyr	-0.542	7.67	-	1	7.7	7.2
pip	-0.506	7.10	-	1	7.1	7.2
mor	-0.493	6.89	-	1	6.9	6.3

Figure 5. (a) Structure of TPMA-based ligands for highly ATRP active Cu/L complexes; (b) comparison of calculated and experimental log k_{act} values. E^{Θ}([Br–Cu^{II}L]$^+$) and experimental log k_{act} values were taken from ref 45, and $\Delta E_{dist,TS}$ from ref 30 C calculated from eq 6. s_C was calculated from eq 8 or approximated to 1 based on the correlation in Figure 4c.

$$\log k_{act} = [-0.622 \times \log \Delta E_{dist,TS} + 1.776] [- 15.9 \times E^{\Theta}([Br - Cu^{II}L]^+) - 0.172 \times BDFE - 0.193 \times EA + 3.44 \times \theta - 0.0529 \times RSE + 8.621 \times \pi^* - 7.864] \quad (9)$$

This equation can be used to calculate k_{act} values of new catalyst–initiator pairs, i.e., when the empirical parameters s_C, C, S, and I are unknown. By utilizing available experimental and computational descriptors, which have been reported in the literature for over 2000 Cu/L-RX pairs, we can greatly expand the scope of the empirical model described in eq 1. However, eq 9 (derived from eq 1) was selected a priori to fit the data set and might not represent the statistically optimal equation for predicting k_{act} using the identified descriptors $\Delta E_{dist,TS}$, E^{Θ}([Br–Cu^{II}L]$^+$), BDFE, EA, RSE, θ, and π^*. Therefore, we developed an alternate model using a more general approach for predicting k_{act}, specifically an MLR approach that is agnostic to any prior assumptions about the relationship between the descriptors and k_{act}. Unlike the application of eq 9, the MLR approach provides a more objective assessment of the descriptors' predictive power. The LFER-based model eq 9 and the MLR model eq 10 were then compared.

2.4. Multivariate Linear Regression. *2.4.1. Construction of the MLR Model.* We performed MLR on the complete set of experimental k_{act} values (98 data points for which the values of all of the descriptors were available), which resulted in the model depicted in Figure 6. Our analysis showed that all of the identified descriptors ($\Delta E_{dist,TS}$, E^{Θ}([Br–Cu^{II}L]$^+$), BDFE, EA, RSE, θ, and π^*) were statistically significant, with p-values of 10^{-4} or lower (as detailed in Table 4, together with the units of measure of each descriptor). In addition to the linear terms, we found that an interaction term between log $\Delta E_{dist,TS}$ and BDFE was statistically significant (p-value $<10^{-5}$). Therefore, we included this interaction term in our model and in the resulting prediction formula. This interaction term strongly mirrors the structure of eq 9, and it agrees with the trends observed for the LFER (Figure 1), whereby Cu/L complexes with markedly different ligand flexibility (i.e., different $\Delta E_{dist,TS}$) exhibit distinctive capability to activate RX with disparate reactivities, resulting in different s_C values.

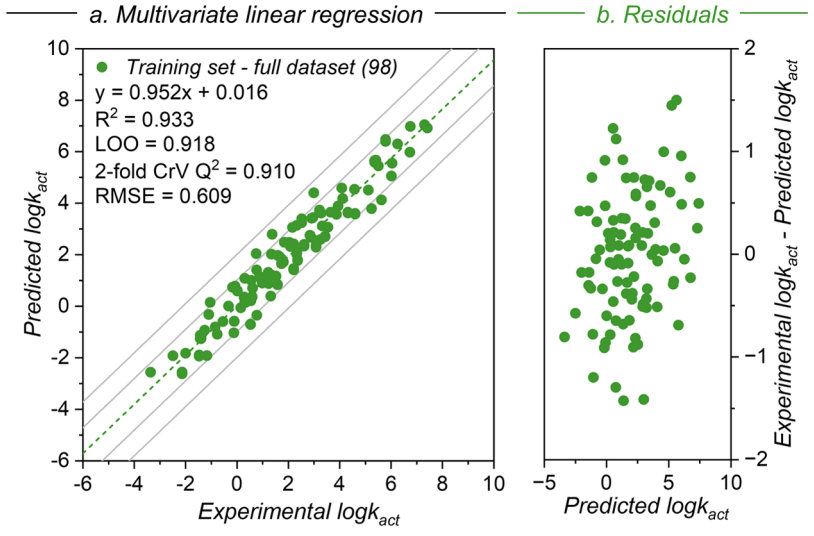

c. Prediction formula

	Electronic effects	Geometric/steric effects	
logk_{act} =	– 10.4 × E^{Θ}([Br-Cu^{II}L]$^+$)	– 2.09 × log$\Delta E_{dist,TS}$	Catalyst-based
	– 0.143 × BDFE – 0.152 × EA + 0.0338 × RSE	+ 2.19 × θ	Initiator-based
	+ 6.85 × π^*		Solvent-based
	+ (log$\Delta E_{dist,TS}$ – 1.39)(BDFE – 246) × 0.0432		Interaction effect
	+ 0.916		

Figure 6. (a) Multidimensional MLR model for ATRP activation, using the full available data set (98 points). The gray lines are added as a visual aid and represent a difference of one and two log units from the linear regression, both in the positive and negative directions. (b) Analysis of the residuals. (c) Subdivision of the prediction equation (eq 10) into electronic and geometric/steric effects.

https://doi.org/10.1021/jacs.3c07711
J. Am. Chem. Soc. 2023, 145, 21587–21599

Table 4. *p*-Values and Percent Contributions to the Multidimensional MLR Model

factor	source	unit of measure	% contribution	*p*-value
$E^{\Theta}([\mathrm{Br{-}Cu^{II}L}]^+)$	catalyst	V vs SCE	17	$<10^{-5}$
$\log \Delta E_{\mathrm{dist,TS}}$		kJ mol^{-1}	4	10^{-4}
θ	RX	rad	4	$<10^{-5}$
RSE		kJ mol^{-1}	5	$<10^{-5}$
BDFE		kJ mol^{-1}	42	$<10^{-5}$
EA		kJ mol^{-1}	18	$<10^{-5}$
$\log \Delta E_{\mathrm{dist,TS}} \times$ BDFE	catalyst−RX interaction	kJ mol^{-1}	4	$<10^{-5}$
π^*	solvent		6	$<10^{-5}$

$$\begin{aligned}\log k_{\mathrm{act}} = {} & -10.4 \times E^{\Theta}([\mathrm{Br} - \mathrm{Cu^{II}L}]^+) \\ & - 2.09 \times \log \Delta E_{\mathrm{dist,TS}} - 0.143 \times \mathrm{BDFE} \\ & - 0.152 \times \mathrm{EA} + 0.0338 \times \mathrm{RSE} + 2.19 \times \theta \\ & + 6.85 \times \pi^* + (\log \Delta E_{\mathrm{dist,TS}} - 1.39) \\ & (\mathrm{BDFE} - 246) \times 0.0432 + 0.916 \end{aligned} \quad (10)$$

The prediction formula for $\log k_{\mathrm{act}}$, eq 10, comprises several electronic as well as geometric and steric effects as summarized in Figure 6c. Table 4 lists the percent contribution of each descriptor to the model; The major contributions are from BDFE and EA of the initiator and from $E^{\Theta}([\mathrm{Br{-}Cu^{II}L}]^+)$.

2.4.2. Validation of the MLR Model. Our developed MLR model was subjected to cross-correlation analysis (Figure S14), which revealed that the descriptors were not significantly intercorrelated. The model showed an excellent quality of fit (R^2 = 0.933, as shown in Figure 6a) and robustness as indicated by cross-validation analyses (leave-one-out (LOO), Q^2 = 0.918, and average-2-fold CrV, Q^2 = 0.910). Additionally, the RMSE associated with the model was low, at 0.609 log units, indicating a satisfactory level of predictive quality. The residual errors appeared randomly distributed (Figure 6b).

2.4.3. Comparison between LFER and MLR Models. The LFER-based model (eq 9) had a lower R^2 value of 0.888 and a higher RMSE of 0.792 (Figure S16) compared to the MLR model (eq 10). This suggests that the MLR model is more accurate for predicting $\log k_{\mathrm{act}}$. Supporting confirmation of the significantly higher predictive power of eq 10 is shown in Figure S17, which suggests that eq 10 is more accurate by about 0.2 log units in predicting $\log k_{\mathrm{act}}$ values, compared to eq 9. Therefore, only the MLR model was further used to calculate unknown $\log k_{\mathrm{act}}$ values, and its predictive power is assessed in detail below.

2.4.4. Assessing the Predictive Power of the MLR Model. To further test the predictive quality of the descriptors, we evaluated whether the MLR model could accurately predict the reactivity of entire classes of substrates that were not included in the original training set. To this end, we repeated the MLR using a training set of 61 data points and three validation sets (37 overall data points), which included the k_{act} values of (i) VCOOMeX (17 data points), which mimics the poly(methyl acrylate) chain end (cf. Scheme 3), (ii) iPCOOEtX (11 data points), which mimic the poly(ethyl methacrylate) chain end, and (iii) VPhX (9 data points), which mimic the polystyrene chain end. The resulting model is presented in Figure 7. Prediction of $\log k_{\mathrm{act}}$ of the validation sets with this model (eq S3 in the SI) resulted in a fit with similar properties to the training set (R^2 between 0.94 and 0.97, and RMSE between 0.25 and 0.54).

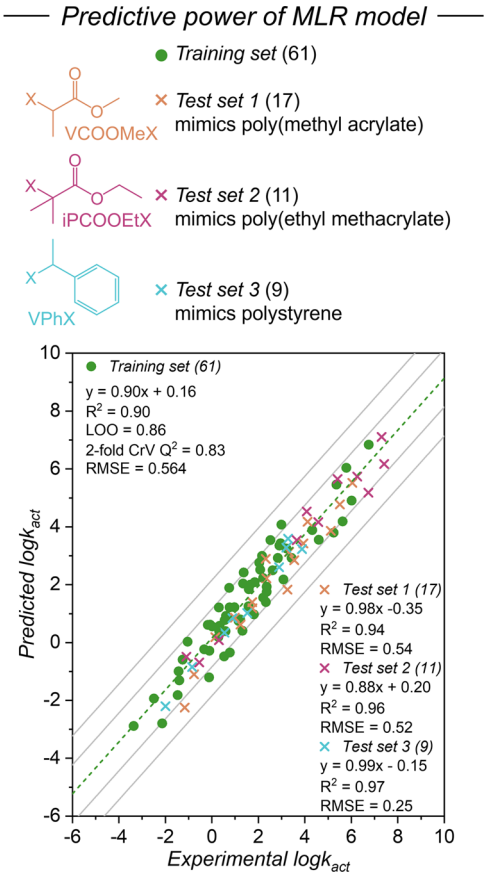

Figure 7. Multidimensional model for $\log k_{\mathrm{act}}$ with training (green dots) and validation data sets (crosses). The values in parentheses indicate the number of data points in each data set.

Given the satisfactory predictive power of the MLR model, eq 10 was used to predict the k_{act} value of ∼2000 new Cu catalyst−initiator pairs (Tables S13 and S14).

2.4.5. Limitations of the MLR Model. The MLR model was generated from a data set that did not include highly sterically hindered catalysts, such as Cu/tris[2-(diethylamino)ethyl]-amine (Cu/Et$_6$TREN). As a result, the model is expected to overestimate the k_{act} values for such catalysts.

The proposed model is highly accurate but rather complex, as it requires 8 parameters. For certain applications, a simpler model might be appropriate. Therefore, a minimal viable model was developed, requiring only 4 easily accessible parameters (E^{Θ}, BDFE, EA, and π^*). The model is presented in Figure S19. This simplified model is less accurate, as can be observed by comparing the output of the statistical tests in Figures 7 and S19, yet it can be useful for estimating the order of magnitude of k_{act} values for new systems with minimal information required.

https://doi.org/10.1021/jacs.3c07711
J. Am. Chem. Soc. 2023, 145, 21587−21599

3. CONCLUSIONS

Linear regression techniques were applied to a large database of activation rate constants k_{act} characterizing the reductive cleavage of C(sp^3)−X bonds in alkyl halides by means of Cu complexes. This database included structurally diverse RX and Cu catalysts typically used in ATRP, and it spanned over 13 orders of magnitude of k_{act} values. The reactivity of these Cu/L-RX pairs was expressed by the simple LFER formula in eq 1: $\log k_{act} = s_C(I + C + S)$. Here, I is the initiator parameter, mainly dictated by the BDFE of RX and by the electron affinity of the halogen radical, and in minor part by the radical stabilization energy of $R^\bullet$ and the Tolman cone angle of RX. C is the catalyst parameter, which correlates with the standard reduction potential of $[Br-Cu^{II}L]^+$. S is the solvent parameter that is linearly correlated to the polarizability of the solvent (π^*). Finally, s_C, the slope of the linear plot, is a catalyst-sensitive parameter, which was determined to correlate linearly with $\Delta E_{dist,TS}$, the distortion energy of Cu/L in its transition state, which primarily depends on the flexibility of L. These descriptors comprehensively describe the reaction of RX activation by Cu/L complexes, a key step in ATRP, as well as in ATRA/C reactions.

Furthermore, an MLR approach was adopted to combine these descriptors in an objective and comprehensive model whereby $\log k_{act}$ is linked to various experimental and computational parameters related to catalysts, initiators, and solvents. The obtained equation was thoroughly validated and subsequently utilized to predict the activity of over 2000 catalyst/initiator pairs in ACN. This predictive model aims to serve as a valuable reference tool for predicting the activity of ATRP systems, and more in general of halogen atom transfer reactions catalyzed by Cu complexes.

In perspective, the data-driven methodology proposed in this work could be adopted to analyze other steps of halogen atom transfer reactions, in particular, the radical deactivation step, which remains the least understood. Moreover, as novel families of "greener" catalysts for ATRP are increasingly gaining attention, such as Fe complexes and organocatalysts, this work is expected to stimulate the collection of significant amounts of data and the consequent use of data-driven approaches to guide the optimization of more sustainable systems for atom transfer radical reactions.

■ ASSOCIATED CONTENT

Supporting Information

The Supporting Information is available free of charge at https://pubs.acs.org/doi/10.1021/jacs.3c07711.

Materials; methods and equipment for the measurement of k_{act} values; library of k_{act} values; additional discussions on parameters; descriptors and validity of the models; and tables with predicted k_{act} values (PDF)

■ AUTHOR INFORMATION

Corresponding Authors

Francesca Lorandi − *Department of Chemistry, Carnegie Mellon University, Pittsburgh, Pennsylvania 15213, United States; Department of Chemical Sciences, University of Padova, Padova 35131, Italy;* orcid.org/0000-0001-5253-8468; Email: francesca.lorandi@unipd.it

Marco Fantin − *Department of Chemical Sciences, University of Padova, Padova 35131, Italy;* orcid.org/0000-0001-9581-2076; Email: marco.fantin@unipd.it

Krzysztof Matyjaszewski − *Department of Chemistry, Carnegie Mellon University, Pittsburgh, Pennsylvania 15213, United States;* orcid.org/0000-0003-1960-3402; Email: matyjaszewski@cmu.edu

Authors

Hossein Jafari − *Department of Chemistry, Carnegie Mellon University, Pittsburgh, Pennsylvania 15213, United States*

Adam Gorczynski − *Department of Chemistry, Carnegie Mellon University, Pittsburgh, Pennsylvania 15213, United States; Faculty of Chemistry, Adam Mickiewicz University, 61-614 Poznań, Poland*

Grzegorz Szczepaniak − *Department of Chemistry, Carnegie Mellon University, Pittsburgh, Pennsylvania 15213, United States; Faculty of Chemistry, University of Warsaw, 02-093 Warsaw, Poland*

Sajjad Dadashi-Silab − *Department of Chemistry, Carnegie Mellon University, Pittsburgh, Pennsylvania 15213, United States;* Present Address: Department of Chemistry, Princeton University, Princeton, New Jersey 08544, United States; orcid.org/0000-0002-4285-5846

Abdirisak A. Isse − *Department of Chemical Sciences, University of Padova, Padova 35131, Italy;* orcid.org/0000-0003-0966-1983

Complete contact information is available at: https://pubs.acs.org/10.1021/jacs.3c07711

Notes

The authors declare no competing financial interest.

■ ACKNOWLEDGMENTS

The support of the U.S. National Science Foundation (NSF, grant CHE 2000391) is gratefully acknowledged. F.L. and M.F. are grateful to Prof. Herbert Mayr and Dr. Manuel Orlandi for fruitful discussions. M.F.'s work was supported by University of Padova (Stars Grant "Photo-e-cat").

■ REFERENCES

(1) Anand, M.; Rohr, B.; Statt, M. J.; Nørskov, J. K. Scaling relationships and volcano plots in homogeneous catalysis. *J. Phys. Chem. Lett.* **2020**, *11* (20), 8518−8526.

(2) Zhao, Z.-J.; Liu, S.; Zha, S.; Cheng, D.; Studt, F.; Henkelman, G.; Gong, J. Theory-guided design of catalytic materials using scaling relationships and reactivity descriptors. *Nat. Rev. Mater.* **2019**, *4* (12), 792−804.

(3) Back, S.; Yoon, J.; Tian, N.; Zhong, W.; Tran, K.; Ulissi, Z. W. Convolutional Neural Network of Atomic Surface Structures To Predict Binding Energies for High-Throughput Screening of Catalysts. *J. Phys. Chem. Lett.* **2019**, *10* (15), 4401−4408.

(4) Steinmann, S. N.; Hermawan, A.; Jassar, M. B.; Seh, Z. W. Autonomous high-throughput computations in catalysis. *Chem. Catal.* **2022**, *2*, 940−956.

(5) Johnson, C. D. Linear free energy relations and the reactivity-selectivity principle. *Chem. Rev.* **1975**, *75* (6), 755−765.

(6) Hammond, G. S. A correlation of reaction rates. *J. Am. Chem. Soc.* **1955**, *77* (2), 334−338.

(7) Michaelides, A.; Liu, Z. P.; Zhang, C. J.; Alavi, A.; King, D. A.; Hu, P. Identification of General Linear Relationships between Activation Energies and Enthalpy Changes for Dissociation Reactions at Surfaces. *J. Am. Chem. Soc.* **2003**, *125* (13), 3704−3705.

(8) Martin, D. J.; Wise, C. F.; Pegis, M. L.; Mayer, J. M. Developing Scaling Relationships for Molecular Electrocatalysis through Studies of Fe-Porphyrin-Catalyzed O2 Reduction. *Acc. Chem. Res.* **2020**, *53* (5), 1056−1065.

(9) Hoffmann, N. M.; Wang, X.; Berkelbach, T. C. Linear Free Energy Relationships in Electrostatic Catalysis. *ACS Catal.* **2022**, *12* (14), 8237−8241.
(10) Schneider, H.-J. Linear free energy relationships and pairwise interactions in supramolecular chemistry. *Chem. Soc. Rev.* **1994**, *23* (4), 227−234.
(11) Williams, A. *Free Energy Relationships in Organic and Bio-Organic Chemistry*; Royal Society of Chemistry, 2003.
(12) Mayr, H.; Kuhn, O.; Gotta, M. F.; Patz, M. Linear free enthalpy relationships: a powerful tool for the design of organic and organometallic synthesis. *J. Phys. Org. Chem.* **1998**, *11* (8−9), 642−654.
(13) Mayr, H.; Patz, M. Scales of nucleophilicity and electrophilicity: a system for ordering polar organic and organometallic reactions. *Angew. Chem., Int. Ed.* **1994**, *33* (9), 938−957.
(14) Mayr, H.; Ofial, A. R. Do general nucleophilicity scales exist? *J. Phys. Org. Chem.* **2008**, *21* (7−8), 584−595.
(15) Orlandi, M.; Escudero-Casao, M.; Licini, G. Nucleophilicity prediction via multivariate linear regression analysis. *J. Org. Chem.* **2021**, *86* (4), 3555−3564.
(16) Mayr's Database of Reactivity Parameters, 2023. https://www.cup.lmu.de/oc/mayr/reaktionsdatenbank2/. (accessed May 02, 2023).
(17) Sigman, M. S.; Harper, K. C.; Bess, E. N.; Milo, A. The Development of Multidimensional Analysis Tools for Asymmetric Catalysis and Beyond. *Acc. Chem. Res.* **2016**, *49* (6), 1292−1301.
(18) Santiago, C. B.; Guo, J.-Y.; Sigman, M. S. Predictive and mechanistic multivariate linear regression models for reaction development. *Chem. Sci.* **2018**, *9* (9), 2398−2412.
(19) Walsh, D. J.; Hyatt, M. G.; Miller, S. A.; Guironnet, D. Recent trends in catalytic polymerizations. *ACS Catal.* **2019**, *9* (12), 11153−11188.
(20) Lorandi, F.; Matyjaszewski, K. Why do we need more active ATRP catalysts? *Isr. J. Chem.* **2020**, *60* (1−2), 108−123.
(21) Wu, C.; Corrigan, N.; Lim, C.-H.; Liu, W.; Miyake, G.; Boyer, C. Rational Design of Photocatalysts for Controlled Polymerization: Effect of Structures on Photocatalytic Activities. *Chem. Rev.* **2022**, *122* (6), 5476−5518.
(22) Matyjaszewski, K.; Tsarevsky, N. V. Macromolecular Engineering by Atom Transfer Radical Polymerization. *J. Am. Chem. Soc.* **2014**, *136* (18), 6513−6533.
(23) Matyjaszewski, K. Advanced materials by atom transfer radical polymerization. *Adv. Mater.* **2018**, *30* (23), No. 1706441.
(24) Lorandi, F.; Fantin, M.; Matyjaszewski, K. Atom Transfer Radical Polymerization: A Mechanistic Perspective. *J. Am. Chem. Soc.* **2022**, *144* (34), 15413−15430.
(25) Tang, W.; Kwak, Y.; Braunecker, W.; Tsarevsky, N. V.; Coote, M. L.; Matyjaszewski, K. Understanding Atom Transfer Radical Polymerization: Effect of Ligand and Initiator Structures on the Equilibrium Constants. *J. Am. Chem. Soc.* **2008**, *130* (32), 10702−10713.
(26) Isse, A. A.; Gennaro, A.; Lin, C. Y.; Hodgson, J. L.; Coote, M. L.; Guliashvili, T. Mechanism of Carbon−Halogen Bond Reductive Cleavage in Activated Alkyl Halide Initiators Relevant to Living Radical Polymerization: Theoretical and Experimental Study. *J. Am. Chem. Soc.* **2011**, *133* (16), 6254−6264.
(27) Braunecker, W. A.; Tsarevsky, N. V.; Gennaro, A.; Matyjaszewski, K. Thermodynamic Components of the Atom Transfer Radical Polymerization Equilibrium: Quantifying Solvent Effects. *Macromolecules* **2009**, *42* (17), 6348−6360.
(28) Gillies, M. B.; Matyjaszewski, K.; Norrby, P.-O.; Pintauer, T.; Poli, R.; Richard, P. A DFT Study of R−X Bond Dissociation Enthalpies of Relevance to the Initiation Process of Atom Transfer Radical Polymerization. *Macromolecules* **2003**, *36* (22), 8551−8559.
(29) Fantin, M.; Isse, A. A.; Bortolamei, N.; Matyjaszewski, K.; Gennaro, A. Electrochemical approaches to the determination of rate constants for the activation step in atom transfer radical polymerization. *Electrochim. Acta* **2016**, *222*, 393−401.
(30) Fang, C.; Fantin, M.; Pan, X.; De Fiebre, K.; Coote, M. L.; Matyjaszewski, K.; Liu, P. Mechanistically guided predictive models for ligand and initiator effects in copper-catalyzed atom transfer radical polymerization (Cu-ATRP). *J. Am. Chem. Soc.* **2019**, *141* (18), 7486−7497.
(31) Pavan, P.; Lorandi, F.; De Bon, F.; Gennaro, A.; Isse, A. A. Enhancement of the Rate of Atom Transfer Radical Polymerization in Organic Solvents by Addition of Water: An Electrochemical Study. *ChemElectroChem* **2021**, *8* (13), 2450−2458.
(32) Horn, M.; Matyjaszewski, K. Solvent Effects on the Activation Rate Constant in Atom Transfer Radical Polymerization. *Macromolecules* **2013**, *46* (9), 3350−3357.
(33) Matyjaszewski, K. Atom Transfer Radical Polymerization (ATRP): Current Status and Future Perspectives. *Macromolecules* **2012**, *45* (10), 4015−4039.
(34) Lin, C. Y.; Marque, S. R. A.; Matyjaszewski, K.; Coote, M. L. Linear-Free Energy Relationships for Modeling Structure−Reactivity Trends in Controlled Radical Polymerization. *Macromolecules* **2011**, *44* (19), 7568−7583.
(35) Isse, A. A.; Bortolamei, N.; De Paoli, P.; Gennaro, A. On the mechanism of activation of copper-catalyzed atom transfer radical polymerization. *Electrochim. Acta* **2013**, *110*, 655−662.
(36) Tang, W.; Matyjaszewski, K. Effects of Initiator Structure on Activation Rate Constants in ATRP. *Macromolecules* **2007**, *40* (6), 1858−1863.
(37) Tang, W.; Matyjaszewski, K. Effect of Ligand Structure on Activation Rate Constants in ATRP. *Macromolecules* **2006**, *39* (15), 4953−4959.
(38) Isse, A. A.; Lorandi, F.; Gennaro, A. Electrochemical approaches for better understanding of atom transfer radical polymerization. *Curr. Opin. Electrochem.* **2019**, *15*, 50−57.
(39) Fantin, M.; Lorandi, F.; Ribelli, T. G.; Szczepaniak, G.; Enciso, A. E.; Fliedel, C.; Thevenin, L.; Isse, A. A.; Poli, R.; Matyjaszewski, K. Impact of Organometallic Intermediates on Copper-Catalyzed Atom Transfer Radical Polymerization. *Macromolecules* **2019**, *52* (11), 4079−4090.
(40) Seeliger, F.; Matyjaszewski, K. Temperature effect on activation rate constants in ATRP: new mechanistic insights into the activation process. *Macromolecules* **2009**, *42* (16), 6050−6055.
(41) Corbin, D. A.; Puffer, K. O.; Chism, K. A.; Cole, J. P.; Theriot, J. C.; McCarthy, B. G.; Buss, B. L.; Lim, C.-H.; Lincoln, S. R.; Newell, B. S.; Miyake, G. M. Radical Addition to N,N-Diaryl Dihydrophenazine Photoredox Catalysts and Implications in Photoinduced Organocatalyzed Atom Transfer Radical Polymerization. *Macromolecules* **2021**, *54* (10), 4507−4516.
(42) Wang, J.-S.; Matyjaszewski, K. Controlled/″ living″ radical polymerization. Halogen atom transfer radical polymerization promoted by a Cu (I)/Cu (II) redox process. *Macromolecules* **1995**, *28* (23), 7901−7910.
(43) Kharasch, M. S.; Jensen, E. V.; Urry, W. Addition of carbon tetrachloride and chloroform to olefins. *Science* **1945**, *102* (2640), 128.
(44) Lanzalaco, S.; Fantin, M.; Scialdone, O.; Galia, A.; Isse, A. A.; Gennaro, A.; Matyjaszewski, K. Atom Transfer Radical Polymerization with Different Halides (F, Cl, Br, and I): Is the Process "Living" in the Presence of Fluorinated Initiators? *Macromolecules* **2017**, *50* (1), 192−202.
(45) Enciso, A. E.; Lorandi, F.; Mehmood, A.; Fantin, M.; Szczepaniak, G.; Janesko, B. G.; Matyjaszewski, K. p-Substituted Tris(2-pyridylmethyl)amines as Ligands for Highly Active ATRP Catalysts: Facile Synthesis and Characterization. *Angew. Chem., Int. Ed.* **2020**, *59* (35), 14910−14920.
(46) Ribelli, T. G.; Lorandi, F.; Fantin, M.; Matyjaszewski, K. Atom Transfer Radical Polymerization: Billion Times More Active Catalysts and New Initiation Systems. *Macromol. Rapid Commun.* **2019**, *40* (1), No. 1800616.
(47) Schröder, K.; Mathers, R. T.; Buback, J.; Konkolewicz, D.; Magenau, A. J. D.; Matyjaszewski, K. Substituted Tris(2-pyridylmethyl)amine Ligands for Highly Active ATRP Catalysts. *ACS Macro Lett.* **2012**, *1* (8), 1037−1040.
(48) Minisci, F. Free-radical additions to olefins in the presence of redox systems. *Acc. Chem. Res.* **1975**, *8* (5), 165−171.

https://doi.org/10.1021/jacs.3c07711
J. Am. Chem. Soc. 2023, 145, 21587−21599

(49) Eckenhoff, W. T.; Pintauer, T. Copper catalyzed atom transfer radical addition (ATRA) and cyclization (ATRC) reactions in the presence of reducing agents. *Catal. Rev.* **2010**, *52* (1), 1−59.
(50) Bengough, W.; Fairservice, W. Effects of salts of metals on vinyl polymerization. Part 1.—Polymerization of methyl methacrylate in presence of cupric chloride. *Trans. Faraday Soc.* **1965**, *61*, 1206−1215.
(51) Bortolamei, N.; Isse, A. A.; Di Marco, V. B.; Gennaro, A.; Matyjaszewski, K. Thermodynamic Properties of Copper Complexes Used as Catalysts in Atom Transfer Radical Polymerization. *Macromolecules* **2010**, *43* (22), 9257−9267.
(52) Hodgson, J. L.; Yeh Lin, C.; Coote, M. L.; Marque, S. R. A.; Matyjaszewski, K. Linear Free-Energy Relationships for the Alkyl Radical Affinities of Nitroxides: A Theoretical Study. *Macromolecules* **2010**, *43* (8), 3728−3743.
(53) Nanda, A. K.; Matyjaszewski, K. Effect of Penultimate Unit on the Activation Process in ATRP. *Macromolecules* **2003**, *36* (22), 8222−8224.
(54) Lin, C. Y.; Coote, M. L.; Petit, A.; Richard, P.; Poli, R.; Matyjaszewski, K. Ab Initio Study of the Penultimate Effect for the ATRP Activation Step Using Propylene, Methyl Acrylate, and Methyl Methacrylate Monomers. *Macromolecules* **2007**, *40* (16), 5985−5994.
(55) Ribelli, T. G.; Fantin, M.; Daran, J.-C.; Augustine, K. F.; Poli, R.; Matyjaszewski, K. Synthesis and Characterization of the Most Active Copper ATRP Catalyst Based on Tris[(4-dimethylaminopyridyl)-methyl]amine. *J. Am. Chem. Soc.* **2018**, *140* (4), 1525−1534.

https://doi.org/10.1021/jacs.3c07711
J. Am. Chem. Soc. 2023, 145, 21587−21599